Analysis of Injection-Locked Pulsed Waveform Oscillators

Mabel Ponton, Elena Fernández, Almudena Suárez, Franco Ramírez
Dpto. de Ingeniería de Comunicaciones
Universidad de Cantabria
Santander, Spain

Abstract— **The injection-locked behaviour of a high efficiency pulsed waveform oscillator is analyzed in detail. The design is based on a closed-loop configuration, loaded with a short nonlinear transmission line (NLTL). A new technique is provided to predict the effect of the circuit elements on the synchronization bandwidth, which enables an overall optimization of the oscillator design, considering efficiency, pulse width and locking interval. The phase-noise minimum in free-running conditions, obtained for particular values of the design parameters, is investigated through the use of phase sensitivity functions. The impact of this minimum on the noise spectrum in injection-locked conditions is also studied. The techniques have been applied to a pulsed-waveform oscillator at 0.9 GHz.**

Keywords: Injection-locking, solitons, oscillators, nonlinear transmission lines, efficiency, phase noise.

I. INTRODUCTION

As shown in several previous works, pulse shaping can be achieved with nonlinear transmission lines (NLTL), usually composed by a high number of inductance-varactor cells [1-2]. The narrow pulses can be applied [3-4] in reflectometry, harmonic generation, signal sampling and ultrawideband communications. They are obtained through the suitable combination of two different effects, the inherent dispersion of the lumped-element line and the nonlinear capacitance $C(v)$ of the varactor diodes, giving rise to a shorter propagation delay for higher voltage amplitude [1-2]. In fact, an input signal with full width at half maximum T_{FWHM} will decompose into $N = 2f_B T_{FWHM}$ individual pulses or solitons, with f_B the Bragg frequency of the NLTL [2]. The individual pulses propagate independently and for higher pulse amplitude, the propagation velocity increases, whereas the T_{FWHM} decreases.

The need for a periodic source at the NLTL input can be eliminated through the design of a free-running soliton oscillator, as shown in the works [3-4]. In [3] a feedback topology is considered, with the NLTL constituting the feedback network of the device used. In [4] the NLTL is the load of a reflection oscillator [4]. The reflection effects enable a reduction of the number of L-varactor cells to about one half of the number used in the feedback configuration. In both cases, the authors use an adaptive bias of the active device to favour one of the pulses while attenuating the others. A different reflection-oscillator design has been proposed in [5], which avoids the need for the adaptive-bias mechanism. It is based on a specific choice of the line elements, enabling a quick formation of the pulsed signal after passing through a small number of NLTL cells. Using the same kind of NLTL design, a high efficiency pulsed-waveform oscillator has been presented in [6]. In that configuration, the NLTL constitutes the load of a feedback Class E oscillator, so the average input impedance exhibited by the NLTL must fit the values required for high efficiency operation. With this kind of design, narrow pulses of about 10% duty cycle were obtained with 48% efficiency. Here the causes for a phase-noise minimum obtained in [6] when varying some critical circuit elements will be investigated using phase-sensitive functions [7]. The relevant aspect of the oscillation start-up and turn-off times, not tackled in [6], is also considered. Unlike [6], the oscillator will be analyzed in injection-locked mode. A new technique enabling an efficient broadening of the synchronization interval will also be presented. The technique, intended for harmonic balance (HB) is of general application to injection-locked oscillators. This optimization technique, valid for small-signal values of the synchronizing source, is applied to the original free-running oscillator design, with no need to obtain the synchronized solution curve resulting from each circuit modification. Therefore, it is computationally very efficient. In this way, it is possible to perform an overall optimization of the oscillator taking into account efficiency, pulse height and width and locking interval. As will be shown, the main advantage of the new pulsed-waveform oscillator configuration is its modularity. In fact, with the particular NLTL design, based on reflection effects, the output pulse duty cycle will keep narrow provided the voltage amplitude at the NLTL input remains sufficiently high. The techniques have been successfully applied to a pulsed waveform oscillator at 0.9 GHz.

II. FREE-RUNNING OSCILLATOR

The oscillator basically consists of a Class E amplifier at the fundamental frequency of the pulsed waveform f_o with a feedback path and loaded with the NLTL. The transistor used is a CLY5. The amplifier output elements (parallel capacitance and series resonant network) are calculated in order to fulfill the zero-voltage switching (ZVS) conditions [8]. The average input impedance of the NLTL, $Z_c = \sqrt{L/C_{eff}}$, with C_{eff} the effective capacitance, must approximately agree with the resistance R_L required for the high-efficiency operation. The pulsed waveform is achieved with a small number of NLTL cells (n=8) using the reflection effects due to the reactive part of the output load. For a fast decomposition of the input wave into individual pulses or solitons, the Bragg frequency

$f_B = 1/(\pi\sqrt{LC_{eff}})$ must not be much higher than the input frequency. This condition is combined with $R_L \cong Z_c$, which leads to the values: f_B=3.2 GHz and L=0.8 nH, with the varactor diode SMV1235. The inductive part of the output load is tuned for a sharp single pulse at the 50 Ohm load. After re-optimization of the overall circuit, the duty cycle is about 10%, with 48% efficiency [6].

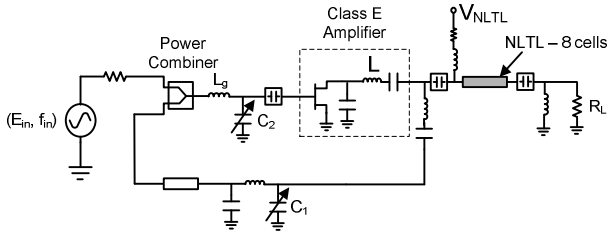

Fig. 1 Schematic of the pulsed-waveform oscillator, containing an amplifier in Class E.

In [6] it was observed that the performance of the pulsed-waveform oscillator was very sensitive to the inductance L (Fig. 2a). In fact, the phase-noise spectral density reached a deep minimum when changing this element, validated with the experimental results. The causes for this minimum were not investigated in [6]. If the phase noise is analyzed suppressing the flicker noise current source, connected in parallel at the drain terminal, the noise minimum is not observed. As shown in [7-9], when using localized models for the noise sources, it is theoretically possible to obtain zero phase-noise contribution of a particular colored source with spectral density $S_{flick,i}(f)$. In fact, the contribution of a particular flicker-noise source $\varepsilon_i(t)$ to the phase-noise spectral density (at sufficiently large offset from the carrier) is given by $S_{p,i}(f) = f_o^2\ b_{dc,i}^2\ S_{flick,i}(f)$ [7], where f_o is the fundamental oscillation frequency, f is the frequency offset and $b_{dc,i}$ is the average value of the phase-sensitivity function $s_i(t)$, associated with the particular flicker-noise source $\varepsilon_i(t)$. This function provides the time derivative of the phase perturbation due to this noise source $\varepsilon_i(t)$, through the expression: $\dot{\theta}(t) = s_i(t)\varepsilon_i(t)$ [7-9]. According to this theory, the absolute value of the average of the sensitivity function $s_i(t)$ should be minimum for L≅4 nH. To verify this, the function $s_i(t)$ has been calculated for different L values. As an example, Fig. 2b shows the sensitive function corresponding to L=2.5 nH and L=3.9 nH. Fig. 2c shows the variation of the average value of $s_i(t)$ versus the inductance L. It crosses zero for L= 4 nH, which approaches the minimum provided by the conversion-matrix approach [10] in Fig. 2a. Discrepancies are attributed to numerical errors in the two different approaches. For explanation, it must be noted that the flicker noise is low frequency and its up-conversion to phase noise depends on the dc component of the sensitivity function, since all the other components will have negligible effect. A resonance effect when changing L may ideally eliminate the dependence of the carrier modulation [10] on the flicker-noise source. In fact, the noise sources are distributed so their contribution cannot be eliminated. However, as confirmed in measurements, the phase noise is noticeably reduced for the inductance value L=3.3 nH.

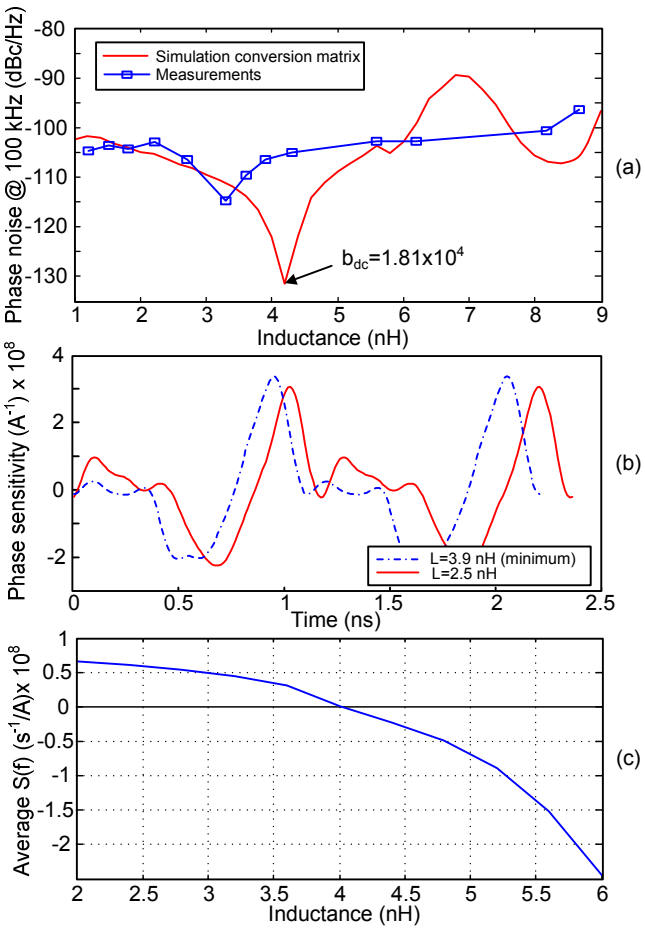

Fig. 2 Phase noise analysis versus L. (a) Phase noise at constant offset frequency 100 KHz. (b) Comparison of the phase sensitivity functions for two L values. (c) Variation of the average S(f).

The start-up and turn off transients of the pulsed-waveform oscillator have also been analyzed. The initial stage of the start-up transient is ruled by the dominant pair of complex-conjugate poles $\sigma \pm j\omega$ of the dc solution, with >0. Then, the transient behavior becomes dependent on the oscillation amplitude and can no longer be predicted with the poles. The turn-off transient is more complex since it involves a big change in the switching element and the dynamics is ruled by the properties of the nonlinear manifolds. When varying the varactor C_1, the turn off transient was extremely long, so this possibility was discarded. When varying the varactor C_2, the turn-off transient was very fast (Fig. 3). On the other hand, provided an additional circuit element can be modified so that σ increases, we should be able to speed up the initial stage of the start-up transient. This analysis has been carried out versus the inductance L_g using pole-zero identification [11] (Fig. 3b). In the two cases, the same two values of varactor bias voltage are considered. For L_g=3 nH we should obtain a transient about three times faster than the one corresponding to the original value L_g=10 nH. This is confirmed by the simulation in Fig. 3a.

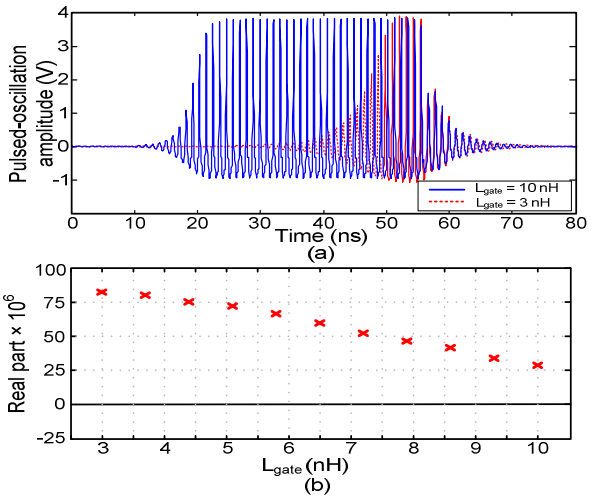

Fig. 3 Transient behavior of the pulsed waveform oscillator versus variations in the varactor C_2. (a) Response for two different L_g values. (b) Variation of the dominant poles of the dc solution versus L_g.

III. Injection-Locked Mode

The injection locking of the pulsed-waveform oscillator will enable control over the oscillation frequency and the pulse position within the oscillation period. It will also be possible to use the circuit as a harmonic generator with very small requirement of RF input power. Here a new technique is presented for the pulsed oscillator optimization, considering the locking bandwidth as one of the performance characteristics, together with the power efficiency and the pulse amplitude. Only the free-running oscillator is modified, taking into account that, provided that the synchronizing source is small signal, the synchronization bandwidth can be estimated linearizing the oscillator circuit about its free-running regime.

The technique is based on the use of an auxiliary generator for the oscillator analysis [12]. The AG is a voltage source connected in parallel at a sensitive circuit node (gate terminal for this analysis), with an ideal bandpass filter, which must fulfill a non-perturbation condition of the oscillatory solution, given by the zero value of the ratio between the current flowing through the generator and the voltage delivered: $Y_{AG}=0$. When solving this condition through optimization, the circuit is analyzed in a two-tier manner, with the pure HB system constituting the inner tier and the condition $Y_{AG}=0$ constituting the outer tier. Then, the synchronization bandwidth will be given by [12-13]:

$$\Delta\omega = \frac{2E_{in}\left|\partial Y_{AG}/\partial E_{in}\right|}{\left|\partial Y_{AG}/\partial\omega\right|\left|\sin(\alpha_{v,\omega})\right|} \qquad (1)$$

where E_{in} is the input generator amplitude and $\alpha_{v,\omega}$ the phase difference between the derivatives $\partial Y_{AG}/\partial\omega$ and $\partial Y_{AG}/\partial V$. Here the partial derivatives are calculated through finite differences in HB using three consecutive sweeps in V, ω and E_{in}, each one starting from the free-running solution, fulfilling $Y_{AG}=0$. For the circuit optimization, we will consider variations in a relevant parameter, for instance the inductance L [14]. At each sweep step, some circuit elements are optimized in order to fulfill the non-perturbation condition $Y_{AG}=0$, which will provide a new free-running solution (this optimization is followed by the three consecutive sweeps). In this manner, it is possible to optimize the injection-locked behavior with no need to obtain the synchronized solution curves at each design modification. Fig. 4 shows the variations of the efficiency, pulse amplitude and synchronization bandwidth versus the inductance L. The bandwidth becomes broader when increasing this inductance but the efficiency decreases and so does the pulse amplitude. The validity of the simulation technique has been verified by tracing the synchronization curves corresponding to L=5.1 nH and 7.9 nH. The measured pulsed waveforms are shown in Fig. 4c.

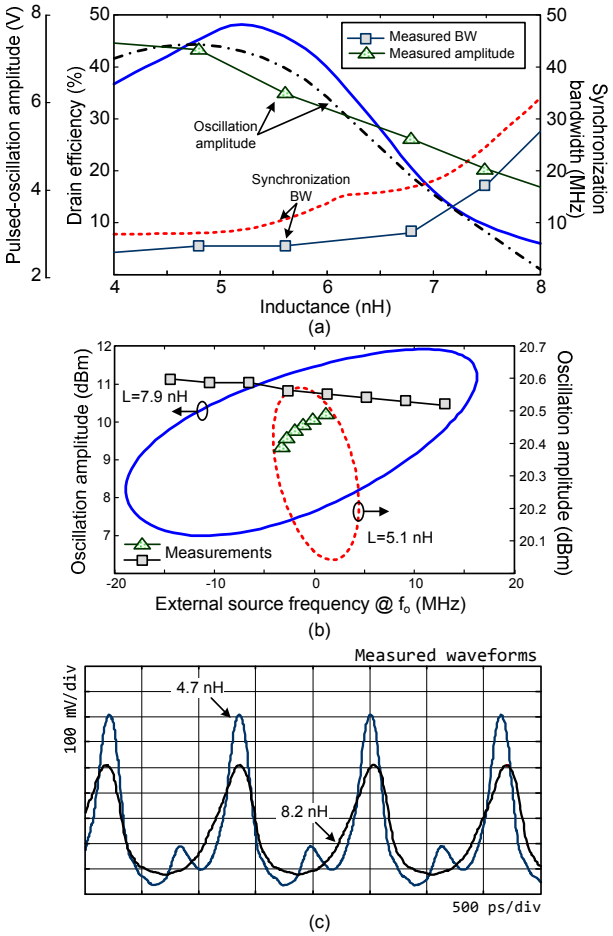

Fig. 4 Optimization of the free-running oscillator at 0.9 GHz attending synchronization bandwidth, efficiency and pulse height. Measurements are superimposed. (a) Variation versus L. (b) Validation with the actual synchronization curves. (c) Experimental pulsed waveform for two L values.

One advantage of the pulse-forming mechanism used here is that the output waveform keeps being a single pulse despite changes in the oscillator elements (other than the NLTL elements). In fact, the output pulse becomes wider and shorter when the amplitude at the NLTL input decreases, but no other pulses appear, that is, we do not get waveforms such as those in previous cells (Fig. 5). Therefore, it is possible to control the overall behavior by simply tracing the pulse amplitude versus the particular analysis parameter, as done in Fig. 3.

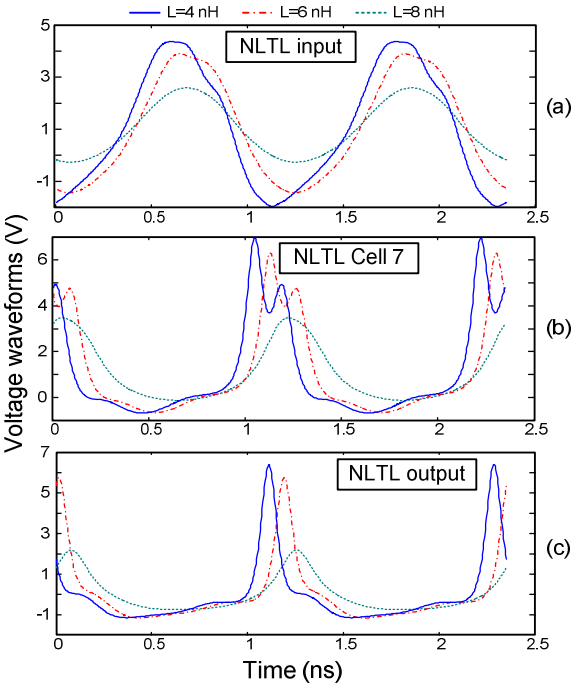

Fig. 5 Voltage waveforms at different circuit locations for three values of the inductance L. (a) NLTL input. (b) Cell 7. (c) NLTL output.

Fig. 6 presents the measured output spectrum in injection-locked conditions obtained for L=6 nH and synchronizing power P_{in}= -16 dBm. As can be seen, the circuit constitutes a good harmonic generator. For the phase noise analysis, the phase-noise spectrum of the synchronizing source has been experimentally characterized and this analysis has been carried out with the conversion matrix approach. In Fig. 7, the spectra obtained for L=3.9 nH and L=6 nH in injection-locked conditions are compared with the one obtained for L=6 nH in free-running regime. When the contribution due to the flicker noise is minimum (L=3.9 nH), the spectrum follows the one corresponding to the input source up to a high offset frequency and the overall phase-noise response is better than the one obtained for L=6 nH. These results are confirmed by the measurements.

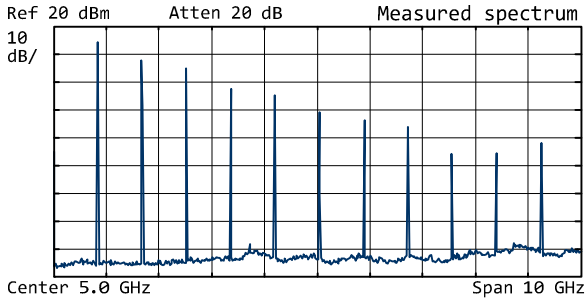

Fig. 6 Measured output spectrum of the pulsed-waveform oscillator in injection-locked conditions.

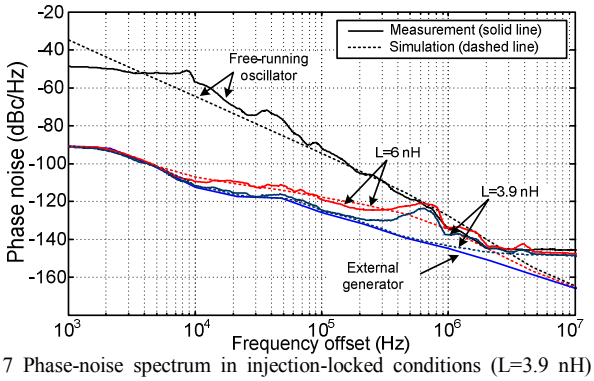

Fig. 7 Phase-noise spectrum in injection-locked conditions (L=3.9 nH) and (L=6 nH) and free-running operation (L=6 nH).

IV. Conclusion

A high efficiency pulsed-waveform oscillator has been analyzed in injection-locked mode. A new simulation technique has been provided to optimize the original free-running oscillator in terms of the power efficiency, pulse amplitude and synchronization bandwidth. Due to the modularity of the design, changes in the oscillator elements have an effect on the pulse amplitude and width but do not give rise to irregular waveforms. The phase-noise spectral density has been analyzed in detail in both free-running and injection-locked conditions.

References

[1] E. Afshari, A. Hajimiri, "Nonlinear Transmission Lines for Pulse Shaping in Silicon", IEEE J. Solid-State Circ., vol. 40, no.3, pp. 744-752 , Mar., 2005.
[2] M. Remoissenet, Waves Called Solitons: Concepts and Experiments, New York: Springer, 1999.
[3] D.S. Ricketts, X.Li, N. Sun, K.Woo,D.Ham, "On the Self-Generation of Electrical solitón Pulses", IEEE J. Solid-State Circuits, vol. 42, no.8 , pp. 1657-1668 , August 2007.
[4] O.O. Yildirim, D. Ricketts, D. Ham, "Reflection Soliton Oscillator", IEEE Trans. Microw. Theory and Tech., vol. 57, no.10, pp. 2344-2353, Oct..2009.
[5] M. Pontón, F.Ramírez, A.Suárez, "Design of pulsed waveform oscillators with a short nonlinear transmission line", IEEE MTT-S Int. Microw. Symp., Anaheim 2010.
[6] M. Pontón, E. Fernández, A. Suárez, F. Ramírez, "Optimized design of pulsed waveform oscillators", IEEE MTT-S Int. Microw. Symp., Baltimore 2011,
[7] A. Demir, "Phase noise and Timig Jitter in oscillators with colored noise sources", IEEE Trans. Circ. and Syst.-I, vol. 49, pp. 1782-1791, Dec. 2002.
[8] N. O. Sokal and F. H. Raab, "Harmonic output of Class-E RF power amplifiers and load coupling network design", IEEE J. Solid-State Circuits, vol. SC-12, no.1, pp. 86-88, Feb. 1977.
[9] S. Sancho, F. Ramirez and A. Suarez, "Analysis and reduction of the oscillator phase noise from the variance of the phase deviations, determined with harmonic balance", IEEE MTT-S, Atlanta (GA), USA, 2008.
[10] V. Rizzoli, F. Mastri, D. Masotti, " General noise analysis of nonlinear microwave circuits by the piecewise harmonic-balance technique", IEEE Trans. on Micro. Theory and Techn., vol. 42, no. 5, pp. 807-819, May. 1994.
[11] J. Jugo, J. Portilla, A. Anakabe, A. Suárez, and J. M. Collantes, "Closed-loop stability analysis of microwave amplifiers", IEE Electronics Letters, vol. 37, pp. 226-228, Feb. 2001.
[12] A. Suárez, *Analysis and Design of Autonomous Microwave Circuits*, Hoboken, New Jersey: Wiley - IEEE Press, 2009.
[13] F. Ramírez, M. Pontón, A. Suárez, "Phase-Noise Analysis of Injected-Locked Oscillators and Analog Frequency Dividers", IEEE Trans. on Microwave Theory and Techn., vol. 56, no.2, pp.393-407, Feb.2008.
[14] H. Zirath, D. B. Rutledge, "An LDMOS VHF Class E Power amplifier using a high Q novel variable inductor", IEEE IMS, California, June,1999.